Am J Physiol Cell Physiol 318: C282–C288, 2020.
First published November 20, 2019; doi:10.1152/ajpcell.00374.2019.

RESEARCH ARTICLE

Gamma oscillations in the pedunculopontine nucleus are regulated by F-actin: neuroepigenetic implications

Francisco J. Urbano,[2] Veronica Bisagno,[3] and Edgar Garcia-Rill[1]

[1]*Center for Translational Neuroscience, University of Arkansas for Medical Sciences, Little Rock, Arakansas;* [2]*Instituto de Investigaciones Farmacológicas, Universidad de Buenos Aires, Buenos Aires, Argentina; and* [3]*Instituto de Fisiología, Biología Molecular, y Neurociencias, Consejo Nacional de Investigaciones Científicas y Técnicas, Universidad de Buenos Aires, Buenos Aires, Argentina*

Submitted 3 September 2019; accepted in final form 20 November 2019

Urbano FJ, Bisagno V, Garcia-Rill E. Gamma oscillations in the pedunculopontine nucleus are regulated by F-actin: neuroepigenetic implications. *Am J Physiol Cell Physiol* 318: C282–C288, 2020. First published November 20, 2019; doi:10.1152/ajpcell.00374.2019.— The pedunculopontine nucleus (PPN) is part of the reticular activating system (RAS) in charge of arousal and rapid eye movement sleep. The presence of high-frequency membrane oscillations in the gamma-band range in the PPN has been extensively demonstrated both in vivo and in vitro. Our group previously described histone deacetylation (HDAC) inhibition in vitro induced protein changes in F-actin cytoskeleton and intracellular Ca^{2+} concentration regulation proteins in the PPN. Here, we present evidence that supports the presence of a fine balance between HDAC function and calcium calmodulin kinase II-F-actin interactions in the PPN. We modified F-actin polymerization in vitro by using jasplakinolide (1 μM, a promoter of F-actin stabilization), or latrunculin-B (1 μM, an inhibitor of actin polymerization). Our results showed that shifting the balance in either direction significantly reduced PPN gamma oscillation as well as voltage-dependent calcium currents.

arousal; calcium channels; calcium currents; gamma oscillations; histone deacetylation; neuroepigenetics; trichostatin A; waking

INTRODUCTION

The pedunculopontine nucleus (PPN) is most active during the two states of arousal, waking, and rapid eye movement sleep (10, 19). The PPN modulates ascending projections through the thalamus influencing arousal and descending projections through the pons and medulla modulating posture and locomotion (11, 19). PPN neuronal activity in the beta/gamma-frequency range has been confirmed in vivo in the cortical EEG and PPN of the cat when the animal is active (33) and in the region of the PPN in humans during stepping but not at rest (12). PPN neurons were found to fire at low frequencies ~10 Hz at rest, but the same neurons increased firing to gamma-band frequencies when the animal woke up or when the animal began walking on a treadmill (13). That is, the same PPN cells were involved in both arousal and motor control.

Recent discoveries have determined the mechanisms behind gamma-band activity in the PPN to be mediated by voltage-dependent, high-threshold N- and P/Q-type Ca^{2+} channels that are expressed in every PPN neuron (10, 11, 14, 15, 19, 20, 35). These Ca^{2+} channel subtypes are modulated by different intracellular pathways: N-type by the cAMP/PK pathway and P/Q-type via the calcium calmodulin kinase II (CaMKII) pathway (9, 23, 24).

Epigenetic mechanisms (i.e., histone posttranslational modification and DNA methylation) play a role in regulation of gene expression in response to a wide range of environmental stimuli, such as learning, stress, or drugs of abuse (4). The recent results of our group showed that *1*) acute in vitro exposure to the histone deacetylation inhibitor trichostatin A (TSA) led to lower activation of high threshold, voltage-dependent Ca^{2+} channel-mediated intrinsic membrane oscillations, specifically in the gamma-band range, but not lower frequency oscillations; *2*) preincubation with TSA led to a similar decrease specifically in gamma-band oscillations; and *3*) a significant reduction in calcium currents was elicited by TSA (11, 34). These changes in PPN rhythmicity could be explained by decreased deacetylation of histones (i.e., changes in gene expression) and/or changes in the deacetylation of other protein targets like CaMKII and F-actin (2, 5). Indeed, proteomic analysis of PPN tissue samples after preincubation (30–60 min, in vitro) with carbachol (CAR) or CAR + TSA showed significant protein changes related to F-actin cytoskeleton and intracellular Ca^{2+} concentration ($[Ca^{2+}]$) regulation (2).

Changes in acetylation of cytoplasmic proteins by histone deacetylation (HDAC) inhibitors have been described, including cytoskeleton-reorganizing proteins (5). We hypothesized that HDAC inhibition of filamentous actin (i.e., F-actin) dynamics may be linked to altered PPN physiology. It has been shown that polymerization of nuclear actin increased histone deacetylase class I (HDAC I) activity (32). At the cytoplasmic level, F-actin interactions with a variety of accessory proteins have been found to be essential for a wide range of dynamic neuronal processes such as axonal growth, synaptic integration, and membrane expression of voltage-dependent channel and their gating (6, 39). Many proteins regulating the turnover of F-actin are Ca^{2+} dependent (27). Depolymerization of F-actin filaments reduced $[Ca^{2+}]$ transients mediated by voltage-dependent Ca^{2+} channels (31). Furthermore, voltage-dependent L-type Ca^{2+} channels mediated Ca^{2+} entry depolymerized F-actin filaments through a PKC-dependent pathway (8). In addition, increasing F-actin depolymerization has been correlated with dendritic spine loss in a mouse model of Alzhei-

Address for reprint requests and other correspondence: E. Garcia-Rill, Center for Translational Neuroscience, Univ. of Arkansas for Medical Sciences, Slot 847, Little Rock, AR 72205 (e-mail: garciarilledgar@uams.edu).

mer's disease (22) and with altered glutamatergic long-term plasticity (25).

Proteomic analysis of PPN tissue samples showed significant protein changes related to F-actin cytoskeleton after acute inhibition of histone deacetylases (2). This study was designed to determine if PPN intrinsic gamma oscillations that are involved in arousal are affected by F-actin polymerization. Herein, we provide novel results on the effects of the histone acetylation inhibitor TSA on F-actin interactions. We studied intrinsic PPN gamma-band oscillatory activity and its underlying changes in Ca^{2+} current density after preincubation with CAR or CAR + TSA. We showed that gamma oscillations in PPN neurons exposed to CAR were indeed modulated by F-actin polymerization. However, preincubation with CAR + TSA blunted F-actin interactions with intrinsic gamma oscillations. These results open important new lines of research on the neuroepigenetics of arousal.

MATERIALS AND METHODS

Animals. All experiments were conducted in compliance with the Animal Research: Reporting of In Vivo Experiments guidelines. Rat pups (n = 36 pups, either sex, aged 9–13 days; 15–23 g) from adult timed-pregnant Sprague-Dawley rats (280–350 g, 6–10 pups per litter) used in this study were provided by the Animal Facility at University of Arkansas for Medical Sciences. Each litter was housed in individually ventilated cages with ad libitum access to water and food. All experimental protocols were approved by the Institutional Animal Care and Use Committee of the University of Arkansas for Medical Sciences (Institutional Animal Care and Use Committee Protocol No. 3906), in agreement with the National Institutes of Health *Guidelines for the Care and Use of Laboratory Animals*.

Slice preparation. Pups were anesthetized with ketamine (70 mg/kg im). The use of ketamine was approved by the Institutional Animal Care and Use Committee of the University of Arkansas for Medical Sciences. When tail pinch reflex was absent, pups were killed by decapitation by a trained researcher and the brain was rapidly removed then cooled in oxygenated sucrose-artificial cerebrospinal fluid (sucrose-aCSF). The sucrose-aCSF consisted of the following (in mM): 233.7 sucrose, 26 $NaHCO_3$, 3 KCl, 8 $MgCl_2$, 0.5 $CaCl_2$, 20 glucose, 0.4 ascorbic acid, and 2 sodium pyruvate. Sagittal sections (400 μm) containing the PPN were cut and slices equilibrated in normal aCSF at room temperature for at least 20 min. The aCSF was composed of the following (in mM): 117 NaCl, 4.7 KCl, 1.2 $MgCl_2$, 2.5 $CaCl_2$, 1.2 NaH_2PO_4, 24.9 $NaHCO_3$, and 11.5 glucose. The recorded neurons were localized in the pars compacta in the posterior PPN, which is easily identified in sagittal sections of the brainstem (19, 20). This area of PPN has been shown to have the highest density of cells (36, 37). We first identified PPN neurons by cell type as previously described (14, 19, 20), although all cell types showed gamma-band oscillations when depolarized using current ramps during recording (17, 18, 20, 34). Slices were recorded at 36°C while perfused (1.5 ml/min) with oxygenated (95% O_2–5% CO_2) aCSF in an immersion chamber for patch-clamp studies as previously described (17, 18, 20, 34).

During recordings, aCSF solution contained the following synaptic receptor antagonists: the selective NMDA receptor antagonist 2-amino-5-phosphonovaleric acid (40 μM; cat. no. A5282, Sigma Aldrich, St. Louis, MO), the competitive AMPA/kainate glutamate receptor antagonist 6-cyano-7-nitroquinoxaline-2,3-dione (10 μM; cat. no. C239, Sigma-Aldrich, St. Louis, MO), the glycine receptor antagonist strychnine (10 μM; cat. no. S0532, Sigma-Aldrich), the specific GABA-A receptor antagonist gabazine (10 μM; cat. no. S106, Sigma-Aldrich), and the nicotinic receptor antagonist mecamylamine (10 μM; cat. no. M9020, Sigma-Aldrich), collectively referred to here as synaptic blockers (SB) plus tetrodotoxin (3 μM; TTX-citrate; cat. no. 554412, Sigma-Aldrich; cat. no. T550, Alomone Laboratories, Jerusalem, Israel; or cat. no. 1069, Tocris, Minneapolis, MN).

Whole cell patch-clamp recordings. Differential interference contrast optics was used to visualize neurons using an upright microscope (Nikon FN-1, Nikon). Whole cell recordings were performed using borosilicate glass capillaries pulled on a P-97 puller (Sutter Instrument Co., Novato, CA) and filled with a high-K^+ intracellular solution, designed to mimic the intracellular electrolyte concentration of the following (in mM): 110 K^+-gluconate, 30 KCl, 10 HEPES, 10 Na_2

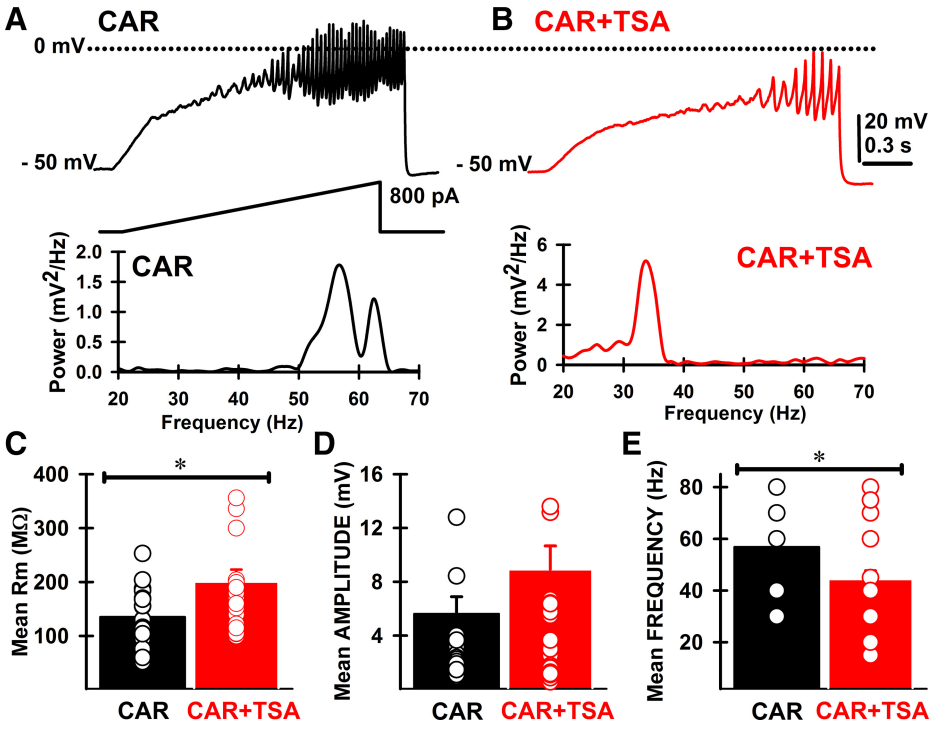

Fig. 1. Effect of in vitro treatment with carbachol (CAR; 50 μM) and CAR + trichostatin A (TSA; 1 μM) on pedunculopontine nucleus (PPN) gamma oscillations. Ramp-induced oscillations (*top*) and power spectrum (*bottom*) from PPN neurons recorded from slices preincubated with either synaptic blockers (SB) + tetrodotoxin (TTX) + CAR (*A*) or SB + TTX + CAR + TSA (*B*). Note higher oscillation frequencies in the power spectrum shown in *A* compared with *B*. *C*: bar graph and individual data (open dots) representing mean input resistance (R_m) for PPN neurons from CAR (black bar; n = 18 PPN cells) and CAR + TSA treatments (red bar; n = 23 PPN cells). *P < 0.05, Student's t test, t = 2.7, df = 39, P = 0.01. *D*: bar graph and individual data (open dots) representing mean amplitude of gamma oscillations for PPN neurons from CAR (black bar; n = 18 PPN cells) and CAR + TSA treatments (red bar; n = 23 PPN cells). *E*: bar graph and individual data (open dots) representing mean frequency of gamma oscillations for PPN neurons from CAR (black bar; n = 18 PPN cells) and CAR + TSA treatments (red bar; n = 23 PPN cells). *P < 0.05, Student's t-test, t = 2.8, df = 39, P = 0.01.

phosphocreatine, 0.2 EGTA, 2 Mg-ATP, 0.5 Li-GTP, and 1 $MgCl_2$. Osmolarity was adjusted to ~270–290 mosM and pH to 7.3. The pipette resistance was 2–5 MΩ. All recordings were made using a Multiclamp 700B amplifier (Molecular Devices, Sunnyvale, CA) in both current- and voltage-clamp mode. Digital signals were low-pass filtered at 2 kHz and digitized at 5 kHz using a Digidata-1440A interface and pClamp10 software (Molecular Devices). We used 1.5 s-long depolarizing current ramps to study membrane potential gamma-band oscillations. Current ramps allow us to gradually change membrane potential from resting values up to 0 mV in current clamp mode (17, 18, 20). Membrane input resistance (R_m) was calculated using square hyperpolarizing current pulses in current-clamp mode (−300 pA, 500-ms long).

PPN slices were recorded after being randomly preincubated with a modified aCSF containing SB + TTX + CAR (50 μM) or SB + TTX + CAR + TSA (CAR + TSA; 1 μM; stock solution prepared in DMSO; Refs. 2, 34). Slices were acutely incubated in either CAR or CAR + TSA-modified aCSF solution from a minimum of 30 min and a maximum of 60 min. Incubation times followed acute periods of incubation previously reported by our group (2, 34). No transcription-translation inhibitor was used during these experiments. Thus acute effects mediated by TSA on PPN rhythmicity could be explained by decreased deacetylation of histones (i.e., changes in gene expression) and/or changes in the deacetylation of other protein targets in the cytoplasm (5). Whole cell patch-clamp recordings were performed in the same modified aCSF that was previously used for preincubation.

The role of F-actin on oscillations was studied using experimental conditions that allowed us to rule out its effects on either Na^+ or T-type voltage-dependent channels (i.e., in the presence of TTX and keeping membrane potential at −50 mV, keeping T-type channels inactivated during experiments; Refs. 14, 20, 23, 24). F-actin polymerization state was studied by adding to the modified saline solutions (CAR or CAR + TSA) jasplakinolide (JAS, 1 μM; an actin-specific reagent that promotes actin polymerization; cat. no. 2792, Tocris) or latrunculin B (LAT-B; 1 μM; an inhibitor of actin polymerization; cat. no. 3974, Tocris). The stock solutions of JAS and LAT-B were dissolved in DMSO and immediately stored at −30°C (the final concentration of DMSO in the incubation aCSF solution was <0.01%). Similar concentrations of JAS and LAT-B have been used by other authors during whole cell patch-clamp recordings in vitro (1, 8, 31, 38).

In addition to membrane oscillation recordings, voltage-dependent Ca^{2+} currents (I_{Ca}) were studied using a high-Cs^+/QX-314 pipette solution (in mM: 110 $CsMeSO_3$, 40 HEPES, 10 TEA-Cl, 12 Na_2-phosphocreatine, 0.5 EGTA, 2 Mg-ATP, 0.5 Li-GTP, and 1 $MgCl_2$. pH was adjusted to 7.3 with CsOH). Cesium and TEA-Cl (cat. no. T2265, Sigma Aldrich) are well-known potassium channel blockers. I_{Ca} was recorded in the presence of extracellular synaptic receptor antagonists and TTX (3 μM) +TEA-Cl (25 mM) (17, 18, 20). Square voltage steps (100-ms long) were used to generate PPN neuronal I_{Ca} from a holding potential of −50 mV, and then depolarized up to 40 mV. Deactivation kinetic (τ) of I_{Ca} was obtained after fitting to a single factor exponential equation: $y = y0 + a \times \exp^{[-\text{Time (ms)}/\tau]}$ individual current deactivation during square pulse depolarization from −50- to 0-mV holding potentials. When fitting r^2 coefficients were <0.8, currents were fitted to a double exponential equation: $y = y0 + a \times \exp^{[-\text{Time (ms)}/\tau 1]} + b \times \exp^{[-\text{Time (ms)}/\tau 2]}$.

Setting the holding potential at −50 mV allowed us to inactivate T-type Ca^{2+} channels, while allowing normal activation of high-threshold P/Q- and N-type Ca^{2+} channels that have been described by our group to mediate PPN membrane potential oscillations (17, 18, 20, 34). Our group has shown that the PPN has three separate populations of neurons that contain either N-type Ca^{2+} channels only (30%), P/Q-type Ca^{2+} channels only (20%), or both N- and P/Q-type Ca^{2+} channels (50%) (23, 24). Here we did not use specific toxins to dissect the specific effects of JAS/LAT-B on N-type expressing PPN neurons. Both series resistance and liquid junction potential were compensated (>14-kHz correction bandwidth; equivalent to <10-ms lag).

Data analysis and statistical comparisons. Off-line analyses were performed using Clampfit software (Molecular Devices, Sunnyvale, CA). Peak oscillatory amplitude was analyzed by first filtering each ramp recording and measuring the three highest amplitude oscillations to derive a mean peak amplitude induced during each ramp. The mean peak frequency of the same three oscillations was filtered and measured to derive a mean frequency of oscillations during the three highest amplitude oscillations in each ramp. The power of each frequency was also analyzed by composing a power spectrum for the frequencies in the entire ramp (bandpass filtered high pass at 10 Hz and low pass at 100 Hz), giving a measure of peak power for frequency (34). Comparisons between groups (control versus 20-min bath application of F-actin modulators) were carried out using OriginPro 9.1.0 (Origin Laboratory.com, Northampton, MA). Normality and equal variance tests were performed before paired, *t* test comparisons using Origin Pro 9.1.0. No sample calculation was performed. Data values that showed >2 SD from the mean were excluded. Differences were considered significant at values of $P \leq 0.05$. Results are presented as means ± SE.

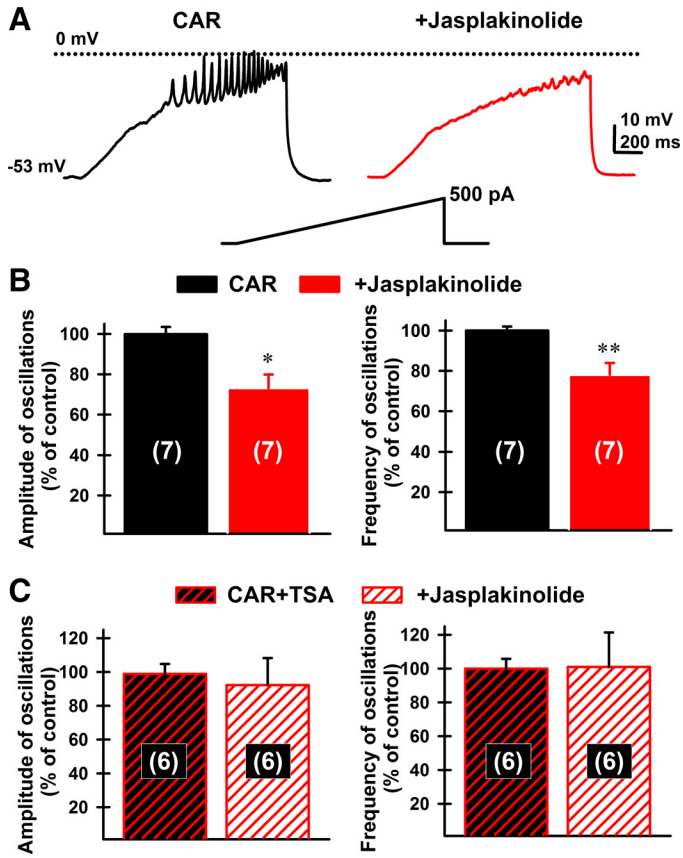

Fig. 2. Effect of in vitro F-actin stabilization with jasplakinolide (JAS; 1 μM) on pedunculopontine nucleus (PPN) gamma oscillations. *A*: ramp-induced oscillations before (black trace) and after bath application of JAS (1 μM; red trace) from a PPN neuron recorded in the presence of synaptic blockers (SB) + tetrodotoxin (TTX) + carbachol (CAR). *B*: bar graphs representing the mean percentage of change of gamma-oscillation amplitude (*left*) and frequency (*right*) for PPN neurons treated with CAR (black bars) or CAR + JAS (solid red bars). *$P < 0.05$, amplitude: paired *t* test, $t = 2.7$, df = 6, $P = 0.02$; **$P < 0.01$, frequency: paired *t* test, $t = 3.6$, df = 6, $P < 0.01$. *C*: same as shown in *B* for PPN neurons treated with CAR + TSA (solid black, red dashed bars) or CAR + TSA + JAS (open, red dashed bars). No statistically different amplitudes (paired *t* test, $t = 0.5$, df = 5, $P = 0.6$) or frequencies (paired *t* test, $t = 0.2$, df = 5, $P = 0.8$) were observed for this treatment group. Numbers in parenthesis in all bar graphs represent the number of cells recorded.

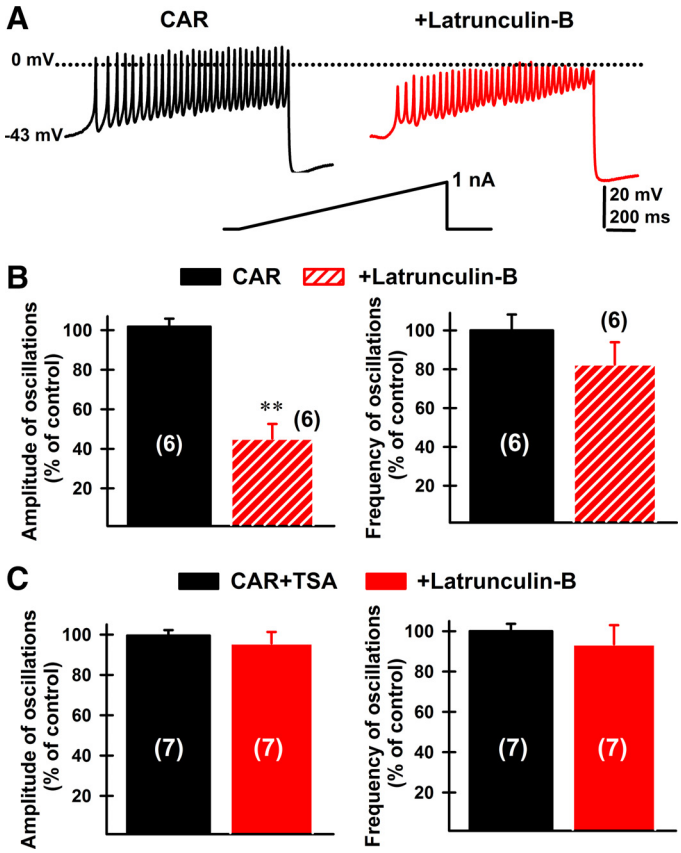

Fig. 3. Effect of in vitro F-actin depolymerization with latrunculin-B (LAT-B; 1 μM) on pedunculopontine nucleus (PPN) gamma oscillations. *A*: ramp-induced oscillations before (black trace) and after bath application of LAT-B (1 μM; red trace) from a PPN neuron recorded in the presence of synaptic blockers (SB) + tetrodotoxin (TTX) + carbachol (CAR). *B*: bar graphs representing the mean percentage of change of gamma-oscillation amplitude (*left*) and frequency (*right*) for PPN neurons treated with CAR (black bars) or CAR + LAT-B (solid, red dashed bars). $^{**}P < 0.01$, amplitude: paired *t* test, $t = 6.8$ df $= 5$ $P < 0.001$; frequency: paired *t* test, $t = 1.3$ df $= 5$ $P = 0.2$. *C*: same as shown in B for PPN neurons treated with CAR + TSA (black bars) or CAR + TSA+LAT-B (solid, red bars). No statistically different amplitudes (paired *t* test, $t = 0.6$, df $= 6$, $P = 0.5$) or frequencies (paired *t* test, $t = 0.5$, df $= 6$, $P = 0.6$) were observed for this treatment group. Numbers in parenthesis in all bar graphs represent the number of cells recorded.

RESULTS

In the present study, we characterized the effects of bath-applied modulators of F-actin polymerization on PPN neuronal rhythmicity and Ca^{2+} currents. Recordings of gamma-band oscillations in PPN neurons (total number of cells studied, $n = 117$; 36 pups) were performed using PPN slices randomly preincubated with a modified saline aCSF solution containing SB + TTX + CAR (i.e., CAR treatment group) or SB + TTX + CAR + TSA (i.e., CAR + TSA treatment group). Throughout this work, we paired recorded PPN cells before and 20 min after JAS (1 μM; an actin-specific reagent that promotes actin polymerization), or LAT-B (1 μM; an inhibitor of actin polymerization).

Initial characterization of PPN neuronal rhythmicity showed that CAR + TSA treatment reduced the frequency of gamma oscillations compared with CAR alone (Fig. 1, *A* and *B*). On average, PPN cells from the CAR + TSA treatment group manifested higher input resistance (R_m; Fig. 1*C*; Student's *t* test, $t = 2.7$, df $= 39$, $P = 0.01$) and lower frequency of oscillations (Fig. 1*E*; Student's *t* test, $t = 2.8$, df $= 39$, $P = 0.01$). No significant differences in mean oscillation amplitude were observed comparing both groups (Fig. 1*D*; Student's *t* test, $t = 0.2$, df $= 39$, $P = 0.9$).

Acute F-actin stabilization with JAS (1 μM) reduced gamma-band oscillations in PPN neurons preincubated with CAR (Fig. 2*A*). In CAR-treated slices, JAS reduced mean amplitude (paired *t* test, $t = 2.7$, df $= 6$, $P = 0.02$) and frequency (paired *t* test, $t = 3.6$, df $= 6$, $P < 0.01$) of gamma oscillations (Fig. 2*B*). However, no significant JAS-mediated effect on either mean amplitude (paired *t* test, $t = 0.5$, df $= 5$, $P = 0.6$) or frequency (paired *t* test, $t = 0.2$, df $= 5$, $P = 0.8$) was observed in cells from the CAR + TSA treatment group.

Acute inhibition of F-actin polymerization with LAT-B reduced the amplitude of gamma-band oscillations in CAR-treated cells (Fig. 3*A*). On average, LAT-B significantly reduced amplitude (paired *t* test, $t = 6.8$, df $= 5$, $P < 0.001$) but not frequency of oscillations (paired *t* test, $t = 1.3$, df $= 5$, $P = 0.2$) in the CAR group (Fig. 3*B*). As was the case with JAS, no effect of LAT-B was observed in the CAR + TSA treatment group (Fig. 3*C*; amplitude: paired *t* test, $t = 0.6$, df $= 6$, $P = 0.5$; frequency: paired *t* test, $t = 0.5$, df $= 6$, $P = 0.6$).

We then tested whether F-actin stabilization affected high-threshold, voltage-dependent Ca^{2+} currents (I_{Ca}). I_{Ca} were recorded after gaining access to the neuronal intracellular space and series resistance was compensated and stable. In CAR-

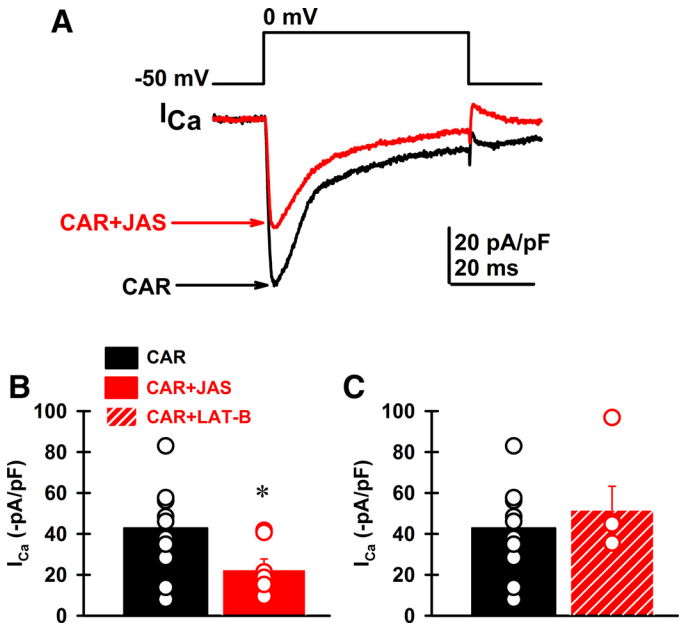

Fig. 4. Effect of in vitro jasplakinolide and latrunculin-B (LAT-B) on pedunculopontine nucleus (PPN) voltage-dependent calcium currents (I_{Ca}). *A*: representative I_{Ca} (current density values, pA/pF) recordings elicited by a 50-ms long depolarizing square step from a holding potential of −50 to 0 mV in a carbachol (CAR)-treated PPN neuron before (black record) and after jasplakinolide (JAS) bath application (red record). *B*: percent change of I_{Ca} amplitude after CAR (black bar) or CAR + JAS (red bar) treatments. *C*: percent change of I_{Ca} amplitude after CAR (black bar) or CAR + LAT-B (dashed red bar) treatments. $^{*}P < 0.05$; comparing CAR vs. CAR + JAS, paired *t* test, $t = 6.6$, df $= 6$, $P < 0.001$. No statistically different I_{Ca}s were observed after CAR + LAT-B bath application (paired *t* test, $t = 1.0$, df $= 4$, $P = 0.4$). Numbers in parenthesis in all bar graphs represent the number of cells recorded.

Table 1. *Effects of JAS and LAT-B on gamma-oscillation-required Ca^{2+}-CAMKII activation*

	CAR + KN93	CAR + KN93 + JAS	CAR + KN93 + LAT-B
Mean amplitude, mV	2.1 ± 0.2 (n = 9)	2.5 ± 0.4 (n = 3)	1.9 ± 0.2 (n = 6)
Mean frequency, Hz	60 ± 4.5 (n = 9)	47 ± 6.7 (n = 3)	58 ± 4.1 (n = 6)

Values are means ± SE. Gamma oscillations were recorded repetitively using up to 3 ramps per pedunculopontine nucleus cell recorded. CAR (50 μM), carbachol; KN93 (1 μM), Ca^{2+}-calcium calmodulin kinase II (CaMKII) inhibitor; JAS (1 μM), jasplakinolide, promotes F-actin polymerization; LAT-B (1 μM), latrunculin-B, inhibitor of F-actin polymerization. No significant differences were observed (t test, $P > 0.05$).

treated slices, bath application of JAS (1 μM) was found to reduce I_{Ca} current density (Fig. 4*A*). In a group of seven PPN neurons, the mean blocking effect on I_{Ca} by JAS was >40% (Fig. 4*B*; paired t test, $t = 6.6$, df = 6, $P < 0.001$). JAS affected I_{Ca} deactivation kinetics during square pulse deactivation. In CAR, I_{Ca} deactivation was fitted to a single exponential function (see MATERIALS AND METHODS), with a mean $\tau = 13.6 \pm 4.5$ ms ($r^2 > 0.9$). However, I_{Ca} recorded in CAR + JAS were best fitted to a double exponential function, yielding $\tau 1 = 26 \pm 8$ ms and $\tau 2 = 6.5 \pm 1.8$ ms ($r^2 > 0.9$). No effect of LAT-B was observed (Fig. 4*C*; paired t test, $t = 1.0$, df = 4, $P = 0.4$) on I_{Ca}.

In CAR + TSA-treated cells, no effects on I_{Ca} were observed after acute bath application of either JAS (paired t test, $t = 2.1$, df = 4, $P = 0.4$), or LAT-B (paired t test, $t = 1.4$, df = 4, $P = 0.2$; data not shown, $n = 5$ PPN cells).

DISCUSSION

We previously described proteomic analysis following in vitro preincubation with CAR or CAR + TSA (2). We observed significant changes particularly in several proteins related to F-actin cytoskeleton and intracellular [Ca^{2+}] regulation in the PPN (2). Other authors have also described fast actions of the HDAC inhibitors SAHA and MS275 on the acetylation of several proteins related to the cytoskeleton (5).

Filamentous actin is a dynamic polymer assembled from ATP-bound G-actin monomers and is a key cytoskeletal component in neuronal dendritic filopodia-like structures and mature dendritic spines (6). F-actin is concentrated in a submembranous region throughout the cell soma (1) as well as in dendritic spines (16). F-actin polymerization dynamics are controlled by the PKC-dependent pathway (8), and, importantly, CaMKII bundles F-actin (28). Under basal conditions, CaMKII is associated with F-actin, while activity-dependent increases in Ca^{2+} levels can disrupt this interaction (21, 28). Exposure to CAR is known to induce gamma oscillations in PPN neurons through the intracellular modulation of P/Q-type Ca^{2+} channels (18) and is a well-known agent for activating PPN (for review, see Ref. 19). It has been established that F-actin acts via CaMKII, an interaction that is finely tuned by intracellular [Ca^{2+}] associated with L-type voltage-dependent Ca^{2+} channels, or NMDA glutamate receptors located at postsynaptic dendritic spines (16). Ca^{2+} entry through NMDA receptors is also reduced after F-actin depolymerization (25). In our study, preincubation of PPN slices with the CaMKII inhibitor KN93 (1 μM) blocked the effects of both JAS and LAT-B on gamma oscillations (Table 1). Although this work includes no experiments using specific toxins to block N-type or P/Q-type calcium channels, our group has reported that KN-93 blocked gamma oscillations and I_{Ca} in PPN neurons expressing P/Q-type channels (~70% of neurons; Refs. 23, 24), suggesting that CaMKII might be interacting with a F-actin-dependent intracellular pathway to modulate P/Q-type channels (9, 23, 24).

JAS is known to modulate the accumulation of disorganized aggregates of F-actin, which would increase the level of spontaneous nucleation sites. This effect may result in disordered polymeric actin, affecting the normal process of actin filament elongation due to the depletion of G-actin monomers (3). Therefore, JAS might be exacerbating F-actin nucleation, which would reduce its ability to anchor voltage-dependent Ca^{2+} channels to the plasma membrane (26), downregulating

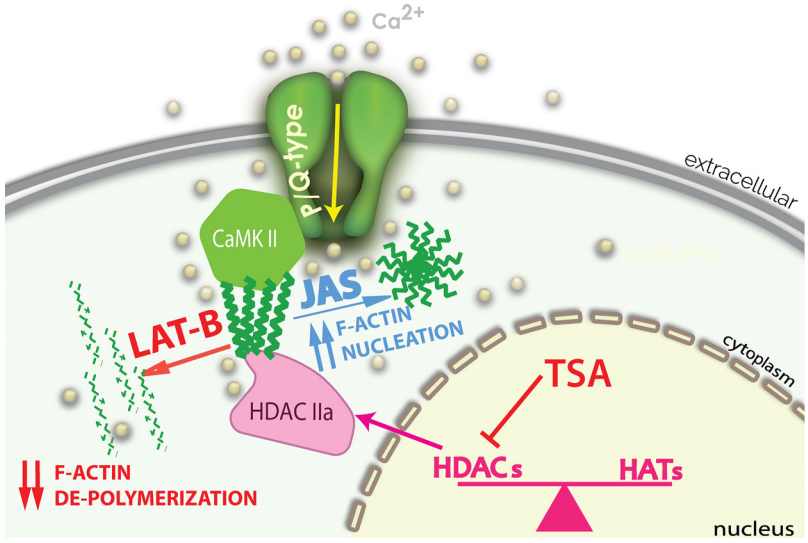

Fig. 5. Schematic summary of the potential relationships between P/Q-type channels, calcium calmodulin kinase II (CaMKII), and F-actin in the presence of histone deacetylase (HDAC) class IIa. P/Q-type calcium channels (green structure) are modulated by CaMKII (green hexagon), which is modulated by HDAC IIa (pink structure), in keeping with our previous findings. Our new results suggest one functional link between HDAC IIa and CaMKII may be F-actin and that shifting the balance towards greater nucleation by using jasplakinolide (JAS) or toward depolymerization using latrunculin-B (LAT-B) would significantly reduce F-actin-CaMKII interactions necessary for gamma-oscillation manifestation. Such interaction would require HDAC-IIa to shuttle out of the nucleus, as previously suggested (11, 34). TSA, trichostatin A; HAT, histone acetyltransferase.

P/Q-type-mediated calcium current density (30), while altering kinetics of T-type calcium channels (29). Such a mechanism would explain the observed reduction in Ca^{2+} current density after bath application of JAS. Our results agree with the previously described amplitude and time course of Ca^{2+}-dependent JAS effects in retinal neurons (31).

Furthermore, we also observed clear effects of both JAS and LAT-B on the mean amplitude of gamma oscillations. These results can be explained by the previously described inhibition of voltage-dependent potassium currents by F-actin depolymerization (31). Preventing F-actin nucleation through Arp2/3 interacting proteins altered inactivation of neuronal potassium channels (39), which represent key intrinsic properties that allow PPN neurons to oscillate at gamma band (20). CaMKII has also been described to modulate these channels, by direct physical association with voltage-dependent, A-type, Kv4 channels (7). Although A-type potassium channels are not involved in gamma oscillations (20), we cannot rule out the existence of CaMKII-mediated modulation of other K^+ channels expressed in PPN neurons. Therefore, F-actin may be changing the dynamics of calcium (29) and potassium channel activation (20, 39) underlying gamma oscillations, leading to decreased amplitude.

In conclusion, we previously determined that HDAC inhibitors affect the interaction between P/Q-type channels and CaMKII, but until now, the mechanistic link between HDAC action and CaMKII was missing. The results herein suggest that at least one of the mechanisms providing a link between histone deacetylation and P/Q-type channel/CaMKII binding is through F-actin. CaMKII is known to bundle F-actin through a stoichiometric interaction, serving as a signaling molecule for such structural changes as dictated by HDACs (28). In keeping with this suggestion, polymerization of nuclear actin increased HDAC activity (32). Figure 5 illustrates potential links between P/Q-type channels, CaMKII, and F-actin, suggesting additional studies to firmly establish these suggestions.

These results do suggest that there is a fine balance between HDAC function and CaMKII-dependent modulation on F-actin. Our results show that shifting the balance F-actin/CaMKII in either direction significantly reduced gamma-oscillation manifestation.

ACKNOWLEDGMENTS

We thank Susan Mahaffey for excellent technical assistance during these experiments.

GRANTS

This work was supported by National Institute of General Medical Sciences Grant P30 GM110702 from the IDeA program (to the Center for Translational Neuroscience, University of Arkansas for Medical Sciences). In addition, this work was supported by grants from FONCYT-Agencia Nacional de Promoción Científica y Tecnológica; Préstamo BID 1728 OC.AR.PICT-2016-1728 and UBACYT 2014-2017 No. 20120130101305BA (to F. J. Urbano); FONCYT-Agencia Nacional de Promoción Científica y Tecnológica; and Préstamo BID 1728 OC.AR.PICT 2015-2594 (to V. Bisagno).

DISCLOSURES

No conflicts of interest, financial or otherwise, are declared by the authors.

AUTHOR CONTRIBUTIONS

F.J.U., V.B., and E.G.-R. conceived and designed research; F.J.U. performed experiments; F.J.U., V.B., and E.G.-R. analyzed data; F.J.U., V.B., and E.G.-R. interpreted results of experiments; F.J.U. prepared figures; F.J.U. and E.G.-R. drafted manuscript; F.J.U., V.B., and E.G.-R. edited and revised manuscript; F.J.U., V.B., and E.G.-R. approved final version of manuscript.

REFERENCES

1. **Akopian A, Szikra T, Cristofanilli M, Krizaj D.** Glutamate-induced Ca^{2+} influx in third-order neurons of salamander retina is regulated by the actin cytoskeleton. *Neuroscience* 138: 17–24, 2006. doi:10.1016/j.neuroscience.2005.11.002.
2. **Byrum SD, Washam CL, Tackett AJ, Garcia-Rill E, Bisagno V, Urbano FJ.** Proteomic measures of gamma oscillations. *Heliyon* 5: e02265, 2019. doi:10.1016/j.heliyon.2019.e02265.
3. **Bubb MR, Spector I, Beyer BB, Fosen KM.** Effects of jasplakinolide on the kinetics of actin polymerization. An explanation for certain in vivo observations. *J Biol Chem* 275: 5163–5170, 2000. doi:10.1074/jbc.275.7.5163.
4. **Cadet JL.** Epigenetics of stress, addiction, and resilience: therapeutic implications. *Mol Neurobiol* 53: 545–560, 2016. doi:10.1007/s12035-014-9040-y.
5. **Choudhary C, Kumar C, Gnad F, Nielsen ML, Rehman M, Walther TC, Olsen JV, Mann M.** Lysine acetylation targets protein complexes and co-regulates major cellular functions. *Science* 325: 834–840, 2009. doi:10.1126/science.1175371.
6. **Coles CH, Bradke F.** Coordinating neuronal actin-microtubule dynamics. *Curr Biol* 25: R677–R691, 2015. doi:10.1016/j.cub.2015.06.020.
7. **Colinas O, Gallego M, Setién R, López-López JR, Pérez-García MT, Casis O.** Differential modulation of Kv4.2 and Kv4.3 channels by calmodulin-dependent protein kinase II in rat cardiac myocytes. *Am J Physiol Heart Circ Physiol* 291: H1978–H1987, 2006. doi:10.1152/ajpheart.01373.2005.
8. **Cristofanilli M, Akopian A.** Calcium channel and glutamate receptor activities regulate actin organization in salamander retinal neurons. *J Physiol* 575: 543–554, 2006. doi:10.1113/jphysiol.2006.114108.
9. **D'Onofrio S, Urbano FJ, Messias E, Garcia-Rill E.** Lithium decreases the effects of neuronal calcium sensor protein 1 in pedunculopontine neurons. *Physiol Rep* 4: e12740, 2016. doi:10.14814/phy2.12740.
10. **Garcia-Rill E, Luster B, D'Onofrio S, Mahaffey S, Bisagno V, Urbano FJ.** Implications of gamma band activity in the pedunculopontine nucleus. *J Neural Transm (Vienna)* 123: 655–665, 2016. doi:10.1007/s00702-015-1485-2.
11. **Garcia-Rill E, D'Onofrio S, Mahaffey SC, Bisagno V, Urbano FJ.** Bottom-up gamma and bipolar disorder, clinical and neuroepigenetic implications. *Bipolar Disord* 21: 108–116, 2019. doi:10.1111/bdi.12735.
12. **Fraix V, Bastin J, David O, Goetz L, Ferraye M, Benabid AL, Chabardes S, Pollak P, Debû B.** Pedunculopontine nucleus area oscillations during stance, stepping and freezing in Parkinson's disease. *PLoS One* 8: e83919, 2013. doi:10.1371/journal.pone.0083919.
13. **Goetz L, Piallat B, Bhattacharjee M, Mathieu H, David O, Chabardès S.** The primate pedunculopontine nucleus region: towards a dual role in locomotion and waking state. *J Neural Transm (Vienna)* 123: 667–678, 2016. doi:10.1007/s00702-016-1577-7.
14. **Garcia-Rill E, Charlesworth A, Heister D, Ye M, Hayar A.** The developmental decrease in REM sleep: the role of transmitters and electrical coupling. *Sleep* 31: 673–690, 2008. doi:10.1093/sleep/31.5.673.
15. **Garcia-Rill E, Luster B, Mahaffey S, MacNicol M, Hyde JR, D'Onofrio SM, Phillips C.** Pedunculopontine gamma band activity and development. *Brain Sci* 5: 546–567, 2015. doi:10.3390/brainsci5040546.
16. **Hell JW.** CaMKII: claiming center stage in postsynaptic function and organization. *Neuron* 81: 249–265, 2014. doi:10.1016/j.neuron.2013.12.024.
17. **Kezunovic N, Hyde J, Simon C, Urbano FJ, Williams DK, Garcia-Rill E.** Gamma band activity in the developing parafascicular nucleus. *J Neurophysiol* 107: 772–784, 2012. doi:10.1152/jn.00677.2011.
18. **Kezunovic N, Hyde J, Goitia B, Bisagno V, Urbano FJ, Garcia-Rill E.** Muscarinic modulation of high frequency oscillations in pedunculopontine neurons. *Front Neurol* 4: 176, 2013. doi:10.3389/fneur.2013.00176.
19. **Kezunovic N, Hyde JR, Urbano FJ, Garcia-Rill E.** Gamma band activity, in *Waking and the Reticular Activating System in Health and Disease* (Garcia-Rill E, editor). New York: Academic, 2015, p. 171–200.
20. **Kezunovic N, Urbano FJ, Simon C, Hyde J, Smith K, Garcia-Rill E.** Mechanism behind gamma band activity in the pedunculopontine nucleus. *Eur J Neurosci* 34: 404–415, 2011. doi:10.1111/j.1460-9568.2011.07766.x.

21. **Khan S, Downing KH, Molloy JE.** Architectural dynamics of CaMKII-actin networks. *Biophys J* 116: 104–119, 2019. doi:10.1016/j.bpj.2018.11.006.
22. **Kommaddi RP, Das D, Karunakaran S, Nanguneri S, Bapat D, Ray A, Shaw E, Bennett DA, Nair D, Ravindranath V.** Aβ mediates F-actin disassembly in dendritic spines leading to cognitive deficits in Alzheimer's disease. *J Neurosci* 38: 1085–1099, 2018. doi:10.1523/JNEUROSCI.2127-17.2017.
23. **Luster B, D'Onofrio S, Urbano F, Garcia-Rill E.** High-threshold Ca^{2+} channels behind gamma band activity in the pedunculopontine nucleus (PPN). *Physiol Rep* 3: e12431, 2015. doi:10.14814/phy2.12431.
24. **Luster BR, Urbano FJ, Garcia-Rill E.** Intracellular mechanisms modulating gamma band activity in the pedunculopontine nucleus (PPN). *Physiol Rep* 4: e12787, 2016. doi:10.14814/phy2.12787.
25. **Meng Y, Zhang Y, Tregoubov V, Janus C, Cruz L, Jackson M, Lu WY, MacDonald JF, Wang JY, Falls DL, Jia Z.** Abnormal spine morphology and enhanced LTP in LIMK-1 knockout mice. *Neuron* 35: 121–133, 2002. doi:10.1016/S0896-6273(02)00758-4.
26. **Mizuno F, Barabas P, Krizaj D, Akopian A.** Glutamate-induced internalization of Ca(v)1.3 L-type Ca(2+) channels protects retinal neurons against excitotoxicity. *J Physiol* 588: 953–966, 2010. doi:10.1113/jphysiol.2009.181305.
27. **Oertner TG, Matus A.** Calcium regulation of actin dynamics in dendritic spines. *Cell Calcium* 37: 477–482, 2005. doi:10.1016/j.ceca.2005.01.016.
28. **Okamoto K, Narayanan R, Lee SH, Murata K, Hayashi Y.** The role of CaMKII as an F-actin-bundling protein crucial for maintenance of dendritic spine structure. *Proc Natl Acad Sci USA* 104: 6418–6423, 2007. doi:10.1073/pnas.0701656104.
29. **Perissinotti PP, Ethington EA, Almazan E, Martínez-Hernández E, Kalil J, Koob MD, Piedras-Rentería ES.** Calcium current homeostasis and synaptic deficits in hippocampal neurons from Kelch-like 1 knockout mice. *Front Cell Neurosci* 8: 444, 2015. doi:10.3389/fncel.2014.00444.
30. **Perissinotti PP, Ethington EG, Cribbs L, Koob MD, Martin J, Piedras-Rentería ES.** Down-regulation of endogenous KLHL1 decreases voltage-gated calcium current density. *Cell Calcium* 55: 269–280, 2014. doi:10.1016/j.ceca.2014.03.002.
31. **Schubert T, Akopian A.** Actin filaments regulate voltage-gated ion channels in salamander retinal ganglion cells. *Neuroscience* 125: 583–590, 2004. doi:10.1016/j.neuroscience.2004.02.009.
32. **Serebryannyy LA, Cruz CM, de Lanerolle P.** A Role for nuclear actin in HDAC 1 and 2 regulation. *Sci Rep* 6: 28460, 2016. doi:10.1038/srep28460.
33. **Steriade M, Paré D, Datta S, Oakson G, Curró Dossi R.** Different cellular types in mesopontine cholinergic nuclei related to ponto-geniculo-occipital waves. *J Neurosci* 10: 2560–2579, 1990. doi:10.1523/JNEUROSCI.10-08-02560.1990.
34. **Urbano FJ, Bisagno V, Mahaffey S, Lee SH, Garcia-Rill E.** Class II histone deacetylases require P/Q-type Ca^{2+} channels and CaMKII to maintain gamma oscillations in the pedunculopontine nucleus. *Sci Rep* 8: 13156, 2018. doi:10.1038/s41598-018-31584-2.
35. **Urbano FJ, D'Onofrio SM, Luster BR, Beck PB, Hyde JR, Bisagno V, Garcia-Rill E.** Pedunculopontine nucleus gamma band activity-preconscious awareness, waking, and REM sleep. *Front Neurol* 5: 210, 2014. doi:10.3389/fneur.2014.00210.
36. **Wang HL, Morales M.** Pedunculopontine and laterodorsal tegmental nuclei contain distinct populations of cholinergic, glutamatergic and GABAergic neurons in the rat. *Eur J Neurosci* 29: 340–358, 2009. doi:10.1111/j.1460-9568.2008.06576.x.
37. **Ye M, Hayar A, Strotman B, Garcia-Rill E.** Cholinergic modulation of fast inhibitory and excitatory transmission to pedunculopontine thalamic projecting neurons. *J Neurophysiol* 103: 2417–2432, 2010. doi:10.1152/jn.01143.2009.
38. **Zhang SX, Duan LH, Qian H, Yu X.** Actin aggregations mark the sites of neurite initiation. *Neurosci Bull* 32: 1–15, 2016. doi:10.1007/s12264-016-0012-2.
39. **Zhang Y, Zhang XF, Fleming MR, Amiri A, El-Hassar L, Surguchev AA, Hyland C, Jenkins DP, Desai R, Brown MR, Gazula VR, Waters MF, Large CH, Horvath TL, Navaratnam D, Vaccarino FM, Forscher P, Kaczmarek LK.** Kv3.3 channels bind hax-1 and arp2/3 to assemble a stable local actin network that regulates channel gating. *Cell* 165: 434–448, 2016. doi:10.1016/j.cell.2016.02.009.